A Universal Density Profile for Cosmic Voids

Nico Hamaus,[1,2,*] P. M. Sutter,[1,2,3] and Benjamin D. Wandelt[1,2,4]

[1] *Sorbonne Universités, UPMC Univ Paris 06, UMR 7095, Institut d'Astrophysique de Paris, F-75014, Paris, France*
[2] *CNRS, UMR 7095, Institut d'Astrophysique de Paris, F-75014, Paris, France*
[3] *Center for Cosmology & AstroParticle Physics, Ohio State University, Columbus, OH 43210, USA*
[4] *Department of Physics, University of Illinois at Urbana-Champaign, Urbana, IL 61801, USA*

(Dated: March 24, 2014)

We present a simple empirical function for the average density profile of cosmic voids, identified via the watershed technique in ΛCDM N-body simulations. This function is universal across void size and redshift, accurately describing the entire radial range of scales around void centers with only two free parameters. In analogy to halo density profiles, these parameters describe the scale radius and the central density of voids. While we initially start with a more general four-parameter model, we find two of its parameters to be redundant, as they follow linear trends with the scale radius in two distinct regimes of the void sample, separated by its compensation scale. Assuming linear theory, we derive an analytic formula for the velocity profile of voids and find an excellent agreement with the numerical data as well. In our companion paper, Sutter al. (2014) [1], the presented density profile is shown to be universal even across tracer type, properly describing voids defined in halo- and galaxy distributions of varying sparsity, allowing to relate various void populations by simple rescalings. This provides a powerful framework to match theory and simulations with observational data, opening up promising perspectives to constrain competing models of cosmology and gravity.

arXiv:1403.5499v1 [astro-ph.CO] 21 Mar 2014

Introduction.—While tremendous efforts have been conducted studying the properties of dark matter halos, cosmic voids have largely been unappreciated by the broad scientific community. However, as voids occupy the most underdense regions in the Universe, and constitute the dominant volume fraction of it, they are promising independent probes to test our theories of structure formation and cosmology. For example, voids are the ideal laboratories for studies of dark energy (e.g., [2–6]) and modified gravity (e.g., [7–10]), as the importance of ordinary gravitating matter is mitigated in their interior. Unlike dark matter halos, voids are in addition more closely related to the initial conditions of the Universe, thanks to the limited number of phase-space foldings occurring inside them [11–13].

A fundamental quantity to describe the structure of voids in a statistical sense is their spherically averaged density profile. In contrast to the well known formulae parameterizing density profiles of simulated dark matter halos (e.g. [14–17]), rather few models for void density profiles have been developed, mainly focusing on the central regions [4, 18–21], rarely taking into account the compensation walls outside the void [22]. In this paper we present a simple formula that is able to accurately describe the density profile around voids of any size and redshift, out to arbitrarily large distance from their center. Although we focus our attention on dark matter simulations here, our companion paper [1] extends the analysis to voids defined in other tracer types, such as dark matter halos and mock galaxies of various number densities, yielding consistent results. Thus, given the excellent agreement between voids found in mocks and in real observations [22–25], our results are relevant for observational data as well.

Simulations.—We analyze outputs of the 2HOT N-body code [26] that evolved 2048^3 cold dark matter particles in a $1h^{-1}$Gpc box of a PLANCK cosmology [27]. The snapshots are randomly sub-sampled to match a mean particle number density of $\bar{n} = 2 \times 10^{-2} h^3 \mathrm{Mpc}^{-3}$, corresponding to an average particle separation of $\bar{r}_\mathrm{p} \simeq 3.7 h^{-1}\mathrm{Mpc}$. This is comparable to the sampling density of modern galaxy surveys, such as [28–30]. We then generate void catalogs using a modified version of the ZOBOV code [4, 23, 31], which finds density minima in a Voronoi tessellation of the tracer particles and grows basins around them by applying the watershed transform [32]. This uncovers a nested hierarchy of voids and sub-voids, all of which we include into our analysis. We restrict ourselves to zones with underdensity barrier $\delta \leq -0.8$ when merging them into voids and define void centers as the mean of the void's particle positions, weighted by their Voronoi cell-volume V_c (see [4, 23]). Finally, an effective void radius r_v is defined as the radius of a sphere comprising the same volume as the watershed region that delimits the void.

Density profile.—We define the void density profile as the spherically averaged relative deviation of mass density around a void center from the mean value $\bar{\rho}$ across the Universe, $\rho_\mathrm{v}(r)/\bar{\rho} - 1$. Using the tracer particles, the density in a radial shell of thickness $2\delta r$ at distance r from a void center at the origin can be estimated as

$$\rho_\mathrm{v}(r) = \frac{3}{4\pi} \sum_i \frac{m_i(\boldsymbol{r}_i)\Theta(r_i)}{(r+\delta r)^3 - (r-\delta r)^3} \,, \qquad (1)$$

where m_i is the mass of particle i, $\boldsymbol{r}_i$ its coordinate vector of length r_i, and $\Theta(r_i) \equiv \vartheta[r_i - (r-\delta r)]\vartheta[-r_i + (r+\delta r)]$ combines two Heaviside step functions ϑ to define the radial bin. In our simulations we use dark matter particles of equal mass and calculate the density profile of every void out to three times its effective radius r_v. In order to avoid contamination from resolution effects, we only include voids with radii larger than twice the mean particle separation $\bar{r}_\mathrm{p}$, and discard density estimates below that scale. We then average (stack) all void profiles within

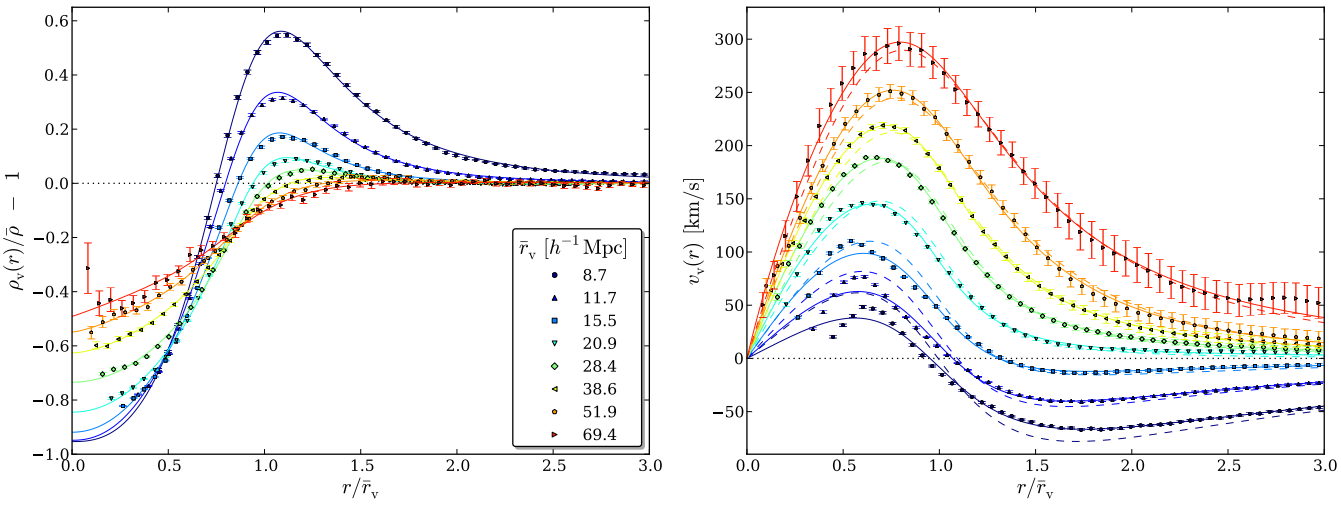

FIG. 1. Stacked density- (left) and velocity- (right) profiles of voids at redshift zero in 8 contiguous bins of void radius with mean values indicated in the inset. Error bars show 68% confidence regions estimated from the standard deviation in each stack, solid lines represent our best-fit solutions to each profile and dashed lines show the linear theory predictions obtained from evaluating the velocity profile at the best-fit parameters obtained from the density stacks.

8 contiguous logarithmic bins in void radius, to account for the poor statistics of the largest voids. The resulting stacks, along with their standard deviations, are shown as symbols with error bars in the left panel of Fig. 1.

As expected, stacked voids are deeply underdense inside, with their central density increasing with void size. In addition, the variance of underdense regions is suppressed compared to overdense ones [33], yielding the smallest error bars in the centers of the emptiest voids. The profiles all exhibit overdense compensation walls, with a maximum located slightly outside their effective void radius, shifting outwards for larger voids. The hight of the compensation wall decreases with void size, causing the inner profile slope to become shallower. This trend divides all voids into being either over- or undercompensated, depending whether the total mass within their compensation wall exceeds or falls behind their missing mass in the center, respectively [34]. Ultimately, at sufficiently large distances to the void center, all profiles approach the mean background density.

We propose a simple empirical formula that accurately captures the properties described above,

$$\frac{\rho_v(r)}{\bar{\rho}} - 1 = \delta_c \frac{1-(r/r_s)^\alpha}{1+(r/r_v)^\beta} \,, \qquad (2)$$

where δ_c is the central density contrast, r_s a scale radius at which $\rho_v = \bar{\rho}$, and α and β determine the inner and outer slope of the void's compensation wall, respectively. The best fits of this four-parameter model to the void density stacks are shown as solid lines in the left panel of Fig. 1. The concordance with the numerical data is exquisite everywhere.

Velocity profile.—We estimate the velocity profile of tracer particles around void centers by calculating

$$v_v(r) = \frac{1}{N(r)} \sum_i \boldsymbol{v}_i(\boldsymbol{r}_i) \cdot \frac{\boldsymbol{r}_i}{r_i} \, V_c(\boldsymbol{r}_i)\Theta(r_i) \,, \qquad (3)$$

for every void and then averaging over all void radii in a given bin. Here, $\boldsymbol{v}_i$ is the particle velocity vector, $V_c(\boldsymbol{r}_i)$ the Voronoi cell volume of a particle located at $\boldsymbol{r}_i$ and $N(r) \equiv \sum_i V_c(\boldsymbol{r}_i)\Theta(r_i)$. Using the Voronoi volumes V_c as weights ensures a volumetric representation of the velocity field [35].

The right panel of Fig. 1 depicts the resulting velocity stacks using the same void radius bins as for the density stacks. Note that a positive velocity implies outflow of tracer particles from the void center, while a negative one denotes infall. As the largest voids are undercompensated (void-in-void [36]), i.e. the total mass in their surrounding does not make up for the missing mass in their interior, they are characterized by outflow in the entire distance range. Tracer velocities increase almost linearly from the void center until they reach a maximum located slightly below the effective void radius of each sample, which indicates the increasing influence of the overdense compensation wall. When passing the latter, tracer velocities are continuously decreasing again in amplitude and approach zero in the large distance limit.

Small voids may exhibit infall velocities, as they can be overcompensated (void-in-cloud [36]). This causes a sign change in their velocity profile around the void's effective radius beyond which matter is flowing onto its compensation wall, ultimately leading to a collapse of the void. Moreover, because small voids are more underdense in the interior, their velocity profile is more nonlinear and less accurately sampled there. The distinction between over- and undercompensation can directly be inferred from velocities, since only overcompensated voids feature a sign change in their velocity profile, while undercompensated ones do not. Consequently, the flow of tracer particles around precisely compensated voids vanishes already at a finite distance to the void center and remains zero outwards. By slightly shifting the void radius bins, we determined this to be the case for voids with

$\bar{r}_\mathrm{v} \simeq 17.6h^{-1}\mathrm{Mpc}$ in our sample, which we denote as the compensation scale. It can also be inferred via clustering analysis in Fourier space, as compensated structures do not generate any large-scale power [34]. We checked that the compensation scales obtained from these two independent methods agree very accurately, indicating a strong link between the spatial and dynamical characteristics of voids.

In linear theory the velocity profile can be related to the density using [37],

$$v_\mathrm{v}(r) = -\frac{1}{3}\Omega_\mathrm{m}^\gamma H(z) r \Delta(r) \,, \tag{4}$$

where Ω_m is the matter content in the Universe, $\gamma \simeq 0.55$ the growth index of matter perturbations, $H(z)$ the Hubble constant and $\Delta(r)$ the integrated density contrast defined as

$$\Delta(r) = \frac{3}{r^3}\int_0^r \left(\frac{\rho_\mathrm{v}(q)}{\bar{\rho}} - 1\right) q^2 \mathrm{d}q \,. \tag{5}$$

With Eq. (2), this integral yields

$$\Delta(r) = \delta_c \, {}_2F_1\!\left(1, \frac{3}{\beta}, \frac{3}{\beta}+1, -(r/r_\mathrm{v})^\beta\right) + \frac{3\delta_c (r/r_s)^\alpha}{\alpha+3} \, {}_2F_1\!\left(1, \frac{\alpha+3}{\beta}, \frac{\alpha+3}{\beta}+1, -(r/r_\mathrm{v})^\beta\right) \,, \tag{6}$$

where ${}_2F_1$ is the Gauss hypergeometric function. When plugged into Eq. (4), we can use this analytic formula to fit the velocity profiles obtained from our simulations, the results are shown as solid lines in the right panel of Fig. 1. As for the density profiles, the quality of the fits is remarkable, especially for large voids. Only the interiors of smaller voids show stronger discrepancy, which is mainly due to the decreasing validity of linear theory, i.e. Eq. (4). We obtain best-fit parameter values that are very similar to the ones resulting from the density stacks above. In fact, evaluating the velocity profile at the best-fit parameters obtained from the density stacks yields almost identical results, as indicated by the dashed lines in Fig. 1.

With the explicit form for the integrated density profile in Eq. (6) it is straightforward to determine the void's uncompensated mass, defined as [34]

$$\delta m = \lim_{r\to\infty} \frac{4\pi}{3}\bar{\rho} r^3 \Delta(r) \,. \tag{7}$$

The limit only exists for $\beta > \alpha + 3$ and yields

$$\delta m = \frac{4\pi^2 \bar{\rho} r_\mathrm{v}^3 \delta_c}{\beta}\left[\csc\left(3\pi/\beta\right) - (r_\mathrm{v}/r_s)^\alpha \csc\left((\alpha+3)\pi/\beta\right)\right] \,, \tag{8}$$

i.e., compensated voids with $\delta m = 0$ satisfy the relation

$$(r_s/r_\mathrm{v})^\alpha = \frac{\sin(3\pi/\beta)}{\sin\left[(\alpha+3)\pi/\beta\right]} \,, \tag{9}$$

independently of δ_c.

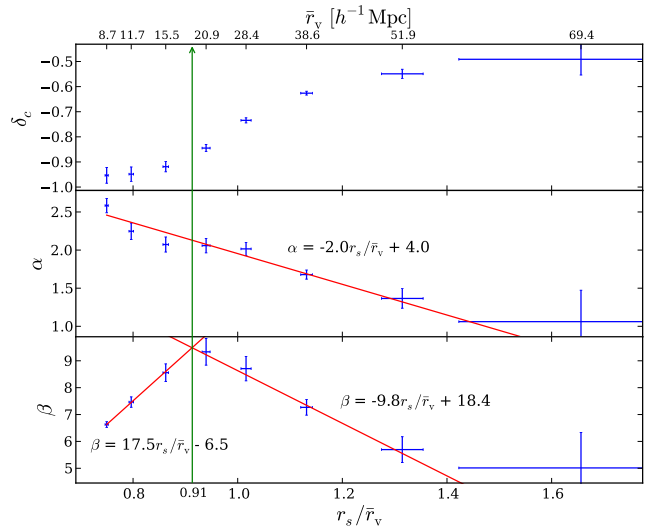

FIG. 2. Best-fit parameters obtained from the density stacks of Fig. 1. Error bars designate 95% confidence regions and straight lines show linear regressions through the data points, with corresponding best-fit values stated alongside. The vertical line indicates the compensation scale of the void sample.

Universality.—Figure 2 depicts the best-fit parameters for each void density stack, where we plot δ_c, α and β against $r_s/\bar{r}_\mathrm{v}$. This representation reveals noticeable correlations among the parameters, which hints at a redundancy of the parameter space. In particular, α exhibits a linear trend with $r_s/\bar{r}_\mathrm{v}$, while β follows a more complicated behavior. However, dividing the void sample into over- and undercompensated voids at $\bar{r}_\mathrm{v} \simeq 17.6h^{-1}\mathrm{Mpc}$, one can approximate β to also follow a linear trend on either side of the vertical line indicating the compensation scale. This can be seen in Fig. 2, where the solid lines result from a linear regression of the corresponding data points, with their explicit linear relations stated aside. They provide a reasonable fit with respect to the size of the error bars. For compensated voids, $r_s/\bar{r}_\mathrm{v} \simeq 0.91$, $\alpha \simeq 2$ and $\beta \simeq 9.5$ attains a maximum. These values precisely satisfy Eq. (9). Even the central density δ_c exhibits a noticeable correlation with $r_s/\bar{r}_\mathrm{v}$, but following a more nonlinear behavior. We therefore do not attempt to express δ_c as a function of $r_s/\bar{r}_\mathrm{v}$ and leave it as a free parameter.

These results suggest the parametrization of Eq. (2) to be overdetermined, and hence the number of free parameters too large for the entire sample of voids. We can plug the best-fit relations

$$\alpha(r_s) \simeq -2\left(r_s/r_\mathrm{v} - 2\right) \,, \tag{10}$$

$$\beta(r_s) \simeq \begin{cases} 17.5 r_s/r_\mathrm{v} - 6.5 & \text{for } r_s/r_\mathrm{v} < 0.91 \\ -9.8 r_s/r_\mathrm{v} + 18.4 & \text{for } r_s/r_\mathrm{v} > 0.91 \,, \end{cases} \tag{11}$$

from Fig. 2 back into Eq. (2) and repeat the fitting procedure for the void stacks in Fig. 1 with the two remaining free parameters δ_c and r_s. This yields fits that are essentially indistinguishable from the original four-parameter model.

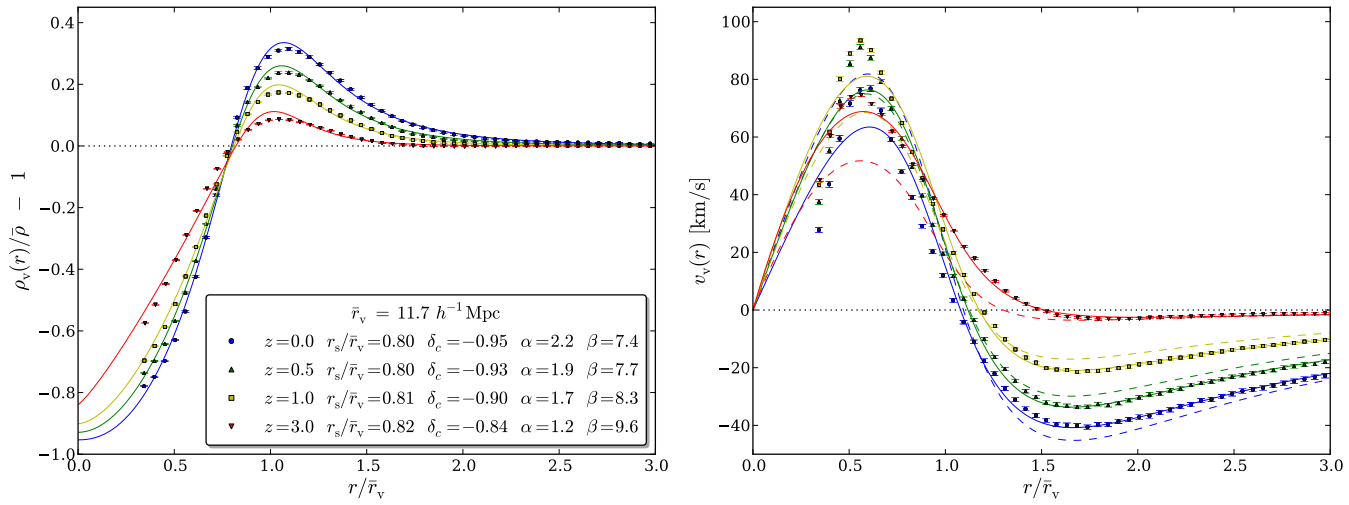

FIG. 3. Same as Fig. 1 for voids of fixed comoving radius at different redshifts as indicated along with the best-fit parameters.

Figure 3 examines the redshift dependence of the density and velocity profile of voids. Here we focus on one of the previous bins with fixed comoving void radius $\bar{r}_v = 11.7h^{-1}$Mpc, representing an overcompensated void. For a first-order approximation, we shall neglect the expansion or contraction of voids that can either leave or enter the bin. As apparent from the left panel, the compensation walls around the void radius grow substantially, while the inner void regions are continuously emptied out, in agreement with theoretical expectations [36]. This is consistent with the evolution of velocities as depicted in the right panel of Fig. 3. Due to its overcompensation, tracer particles outside the void build up higher and higher velocities towards the void center, which causes the compensation wall to grow. Inside the void the outflow also first increases at high redshift, but as the Universe accelerates its expansion after the onset of dark energy domination ($z \sim 1$), this trend reverses and the outflow is attenuated.

Solid lines in Fig. 3 represent the best-fit solutions of Eqs. (2), (4) and (6) to the data, the corresponding parameters for the density profile are shown in the figure inset. The excellent agreement even at higher redshifts indicates a universal behavior of these empirical formulae. We also repeated our analysis based on a WMAP7 cosmology [38], finding fully consistent results. Moreover, in this paper we neglected the impact of redshift-space distortions, since void density profiles can be reconstructed in real space when statistical isotropy is assumed [25]. Nevertheless, we find redshift-space distortions to just mildly affect the profile shapes of voids, barely degrading the quality of our fits.

Discussion.—There are a number of cosmological applications to make use of the presented functional form of the average void density profile. For example, studies of gravitational (anti-) lensing that directly probe the projected mass distribution around voids [39–42], which in turn may serve as a tool for constraining models of dark matter, dark energy and modified gravity. But also considering galaxy surveys, an accurate model for the void density profile can aid in measuring the Alcock-Paczynski effect [4, 43, 44] and the Integrated Sachse-Wolfe effect [2, 6, 10, 45, 46], for example. This is thanks to the universal nature of Eq. (2), which even describes voids in the distribution of galaxies remarkably well, as demonstrated in [1]. With that, clustering analyses based on the void model [34] can directly make use of the analytical form of the density profile for voids. In [1] it is further pointed out that the impact of tracer sparsity and bias on the definition of voids can be accounted for by simple rescaling of void sizes. These findings corroborate other indications that cosmic voids may indeed offer new and complementary approaches to modeling fundamental aspects of the large-scale structure of our Universe.

We thank Michael Warren for providing his N-body simulations and Jens Jasche, Guilhem Lavaux, Florent Leclercq, Mark Neyrinck, Alice Pisani, Ravi Sheth, Joe Silk and Rien van de Weygaert for discussions. This work made in the ILP LABEX (under reference ANR-10-LABX-63) was supported by French state funds managed by the ANR within the Investissements d'Avenir program under reference ANR-11-IDEX-0004-02. This work was also partially supported by NSF AST 09-08693 ARRA. B.D.W. is supported by a senior Excellence Chair by the Agence Nationale de Recherche (ANR-10-CEXC-004-01) and a Chaire Internationale at the Université Pierre et Marie Curie.

* hamaus@iap.fr

[1] P. M. Sutter, G. Lavaux, N. Hamaus, B. D. Wandelt, D. H. Weinberg, and M. S. Warren, Mon. Not. R. Astron. Soc. submitted (2014), 1309.5087.
[2] B. R. Granett, M. C. Neyrinck, and I. Szapudi, Astrophys. J. **683**, L99 (2008).
[3] R. Biswas, E. Alizadeh, and B. D. Wandelt, Phys. Rev. D **82**, 023002 (2010).
[4] G. Lavaux and B. D. Wandelt, Astrophys. J. **754**, 109

(2012).
[5] E. G. P. Bos, R. van de Weygaert, K. Dolag, and V. Pettorino, Mon. Not. R. Astron. Soc. **426**, 440 (2012).
[6] Y.-C. Cai, M. C. Neyrinck, I. Szapudi, S. Cole, and C. S. Frenk, ArXiv e-prints (2013), 1301.6136.
[7] B. Li, Mon. Not. R. Astron. Soc. **411**, 2615 (2011).
[8] J. Clampitt, Y.-C. Cai, and B. Li, Mon. Not. R. Astron. Soc. **431**, 749 (2013).
[9] D. Spolyar, M. Sahlén, and J. Silk, Phys. Rev. Lett. **111**, 241103 (2013).
[10] Y.-C. Cai, B. Li, S. Cole, C. S. Frenk, and M. Neyrinck, Mon. Not. R. Astron. Soc. (2014).
[11] M. C. Neyrinck, Mon. Not. R. Astron. Soc. **427**, 494 (2012).
[12] M. C. Neyrinck and L. F. Yang, Mon. Not. R. Astron. Soc. **433**, 1628 (2013).
[13] F. Leclercq, J. Jasche, H. Gil-Marín, and B. Wandelt, J. Cosmol. Astropart. Phys. **11**, 048 (2013).
[14] J. Einasto, Trudy Astrofizicheskogo Instituta Alma-Ata **5**, 87 (1965).
[15] A. Burkert, Astrophys. J. **447**, L25 (1995).
[16] J. F. Navarro, C. S. Frenk, and S. D. M. White, Astrophys. J. **490**, 493 (1997).
[17] B. Moore, T. Quinn, F. Governato, J. Stadel, and G. Lake, Mon. Not. R. Astron. Soc. **310**, 1147 (1999).
[18] J. M. Colberg, R. K. Sheth, A. Diaferio, L. Gao, and N. Yoshida, Mon. Not. R. Astron. Soc. **360**, 216 (2005).
[19] N. D. Padilla, L. Ceccarelli, and D. G. Lambas, Mon. Not. R. Astron. Soc. **363**, 977 (2005).
[20] E. Ricciardelli, V. Quilis, and S. Planelles, Mon. Not. R. Astron. Soc. **434**, 1192 (2013).
[21] E. Ricciardelli, V. Quilis, and J. Varela, Mon. Not. R. Astron. Soc. (2014), 1402.2976.
[22] D. Paz, M. Lares, L. Ceccarelli, N. Padilla, and D. G. Lambas, Mon. Not. R. Astron. Soc. **436**, 3480 (2013).
[23] P. M. Sutter, G. Lavaux, B. D. Wandelt, and D. H. Weinberg, Astrophys. J. **761**, 44 (2012).
[24] P. M. Sutter, G. Lavaux, B. D. Wandelt, D. H. Weinberg, and M. S. Warren, ArXiv e-prints (2013), 1310.7155.
[25] A. Pisani, G. Lavaux, P. M. Sutter, and B. D. Wandelt, ArXiv e-prints (2013), 1306.3052.
[26] M. S. Warren, in *Proceedings of SC13: International Conference for High Performance Computing, Networking, Storage and Analysis* (ACM, New York, NY, USA, 2013), SC '13, pp. 72:1–72:12.
[27] Planck Collaboration, P. A. R. Ade, N. Aghanim, C. Armitage-Caplan, M. Arnaud, M. Ashdown, F. Atrio-Barandela, J. Aumont, C. Baccigalupi, A. J. Banday, et al., ArXiv e-prints (2013), 1303.5076.
[28] *SDSS*, URL `http://www.sdss.org/`.
[29] *DES*, URL `http://www.darkenergysurvey.org`.
[30] *EUCLID*, URL `http://sci.esa.int/euclid`.
[31] M. C. Neyrinck, Mon. Not. R. Astron. Soc. **386**, 2101 (2008).
[32] E. Platen, R. van de Weygaert, and B. J. T. Jones, Mon. Not. R. Astron. Soc. **380**, 551 (2007).
[33] F. Bernardeau, C. Pichon, and S. Codis, ArXiv e-prints (2013), 1310.8134.
[34] N. Hamaus, B. D. Wandelt, P. M. Sutter, G. Lavaux, and M. S. Warren, Phys. Rev. Lett. **112**, 041304 (2014).
[35] Note1, we thank Guilhem Lavaux for pointing this out.
[36] R. K. Sheth and R. van de Weygaert, Mon. Not. R. Astron. Soc. **350**, 517 (2004).
[37] P. J. E. Peebles, *Principles of Physical Cosmology* (1993).
[38] E. Komatsu, K. M. Smith, J. Dunkley, C. L. Bennett, B. Gold, G. Hinshaw, N. Jarosik, D. Larson, M. R. Nolta, L. Page, et al., ApJS **192**, 18 (2011).
[39] K. Bolejko, C. Clarkson, R. Maartens, D. Bacon, N. Meures, and E. Beynon, Phys. Rev. Lett. **110**, 021302 (2013).
[40] Y. Higuchi, M. Oguri, and T. Hamana, Mon. Not. R. Astron. Soc. **432**, 1021 (2013).
[41] E. Krause, T.-C. Chang, O. Doré, and K. Umetsu, Astrophys. J. **762**, L20 (2013).
[42] P. Melchior, P. M. Sutter, E. S. Sheldon, E. Krause, and B. D. Wandelt, ArXiv e-prints (2013), 1309.2045.
[43] C. Alcock and B. Paczynski, Nature **281**, 358 (1979).
[44] P. M. Sutter, G. Lavaux, B. D. Wandelt, and D. H. Weinberg, Astrophys. J. **761**, 187 (2012).
[45] S. Ilić, M. Langer, and M. Douspis, A&A **556**, A51 (2013).
[46] C. Hernández-Monteagudo and R. E. Smith, Mon. Not. R. Astron. Soc. **435**, 1094 (2013).